DNS and LDA-measurements in the near wake of a blunt-trailing-edged body

Eduardo Silveira Molina, molina@ita.br
Marcos Aurélio Ortega, ortega@ita.br
Roberto da Motta Girardi, girardi@ita.br
ITA - Technological Institute of Aeronautics, São José dos Campos, SP, 12228-900, Brasil

Abstract. *An investigation of the near wake at the base of a blunt-trailing-edged body is attempted with the help of a Direct Numerical Simulation (DNS) numerical tool together with the Laser Doppler Anemometry (LDA) technique. This work is a natural experimental extension of a former numerical research by the present group of authors. The near wake region is investigated in 2-D (DNS), 3-D (DNS) and 3-D (LDA). The aim is directed towards the understanding of the physical mechanisms and the differences between both approaches. It is known that, what happens in this region is decisive to the characteristics of the downstream wake. Statistical moments are presented for the streamwise and cross-wise velocity components, respectively. Other studies show good agreement of the Strouhal number and a disagreement of some important length scales (formation region and wake closure).*

Keywords: *bluff body, near wake, DNS and LDA*

1. INTRODUCTION

The formation of vortex structures in the wake of bluff bodies has been the subject of intense study of engineers and scientists for almost a century. It is well known that the physics of this type of flow represents a great challenge to the analyst. Much of this work has focused on the circular cylinder, owing in part to the geometrical symmetry, simplicity, and engineering practicality (Roshko, 1954a; Bloor, 1964; Gerrard, 1966; Williamson, 1996; to name but only a few).

The alternate shedding of vortices in the near wake of a bluff body, leads to an increase in the mean drag, lift and pressure fluctuations, and may cause structure vibration, acoustic noise, or resonance, which in some cases can trigger failure processes (Williamson, 1996).

Over a century ago, Strouhal (1878) studied the vortex shedding from a cylinder and demonstrated that its dimensionless frequency (fD/U) remained constant over a range of Reynolds number (DU_∞/ν) . The basic analysis of the flow wake was pioneered by von Kármán's classical work. He established a theoretical link between the vortex street structure and the drag on the body. The author found that two symmetric or anti-symmetric vortex rows of opposite sign were physically unstable, with the exception of only one specific configuration which exhibited neutral stability, and for which $b/a = 0.28056$, where b = inter-vortex spacing in one row and a = distance between vortex rows.

Fage and Johansen (1928) measured the thickness of the free shear layer of different bluff bodies. The authors noticed the existence of very low flow velocities behind the body, given the name of "dead-air" region. Another important statement of the authors was that the vorticity rate shed at the upper and lower separation points for both symmetric and antisymmetric bodies had approximately the same value. In spite of that, there is a decreased in the vorticity rate throughout the wake due to entrainment of fluid from outside of the wake and a interaction between the upper and lower free shear layers in the formation region.

Particularly, the plot of the base pressure coefficient (C_{pb}) as function of the Reynolds number reveals important changes in the flow structure for different flow regimes. If all or even part of the available data were shown on this plot, there would be considerable dispersion, and this even for smooth cylinders at low levels of turbulence. As it is well known, the free-stream turbulence amplitude and cylinder roughness tend to trigger the transition at lower ranges of the Reynolds number (Roshko, 1993).

One of the main interpretations for the near wake vortex formation was given by Gerrard (1996). He proposed that a forming vortex draws the shear layer of opposite sign from the other side of the wake, eventually cutting off the supply of vorticity to the growing vortex, therefore precipitating the structure shedding downstream.

Due to the induced velocities by the growing vortex behind the body, in the so-called "dead-air" region, the ratio of the local velocity to the free-stream velocity is almost zero, leading to low values of C_{pb}. According to Fage and Johansen (1928), the base pressure coefficient is directly related to the velocity on the separation point, and this relationship is given by:

$$C_{pb} = 1 - \left(\frac{U_s}{U_\infty}\right)^2 \tag{1}$$

$$C_{pb} = 1 - K^2 \tag{2}$$

where U_∞ is the free stream velocity, U_S is the separation point velocity and K is the ratio between both.

The first definition of flow regimes based on measurements of velocity fluctuations, spectra and frequency, was given

by Roshko (1954b). After that much has been done in the area, with some discrepancies appearing in the measurements due both to differences in experimental conditions as well as to the ever present three-dimensional effects.

Roshko (1993), in his review, stated that one of the most problematic aspects of bluff bodies comes exactly from effects of three dimensionality, in other words, the appearance of three dimensional motions in what is nominally a two dimensional flow. Some influences at the wind tunnel environment are, say, extrinsic, in particular, end plate effects in conjunction with the aspect ratio, Szepessy and Bearman (1992). The other are intrinsic and related to the specificities of the three-dimensional natural instabilities: the just-released two-dimensional roll hairpin effect or the instability at the braids between rolls (Williamson, 1996).

Differently from the cylinder, geometries like the flat plate, wedge and blunt-trailing-edges bodies have fixed separation points at which the flow suddenly changes from a boundary layer flow to the wake.

2. ESTABLISHMENT OF THE PROBLEM

One wishes to investigate experimentally and simulate numerically the two-dimensional flow of an incompressible fluid about a bluff body as shown in Fig. 1 and Tab. 1. The body consists of an elliptic nose section followed by a parallel-sided section. The chord and the base height are indicated by c and h, respectively. Thus, the aspect ratio, AR, is defined by c/h. L_x is the length while L_y is the width of the domain. The position of the central chord is fixed by x_c and y_c. The distance between the body vertical wall and the exit of domain is indicated by q. Finally, the angle of attack is zero.

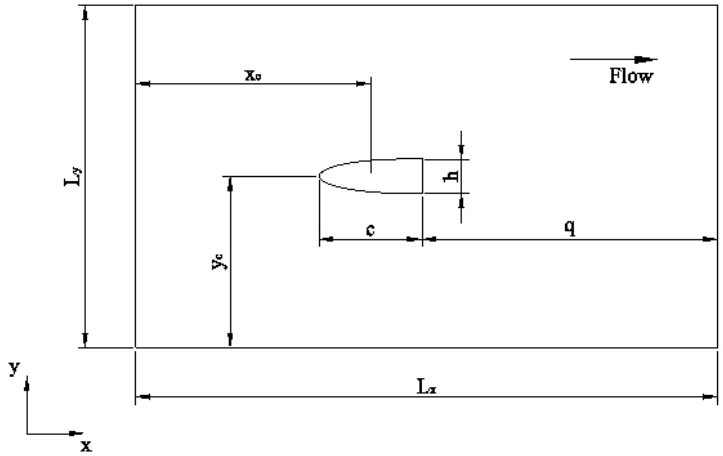

Figure 1: Computational and experimental domain

	L_y	L_x	y_c	x_c	q
DNS	$15h$	$30h$	$7.5h$	$13.5h$	$15h$
LDA	$9.8h$	$19h$	$5.9h$	$7.5h$	$10h$

Table 1: Data relative to the computational and experimental domain.

The values of the aspect ratios chosen for the numerical and experimental studies are: $AR = 3$, $AR = 5$ and $AR = 7$. The front part of the elliptic nose section was fixed relative to the $AR = 3$ configuration, with semi-major and semi-minor axes of $5c/6$ and $h/2$, respectively, followed by a parallel-sided section of length $c/6$. For the other two bodies, the same elliptical nose was maintained, while the length of the afterbody was varied according to the desired aspect ratio. The reason for keeping those overall proportions is because the resulting flow is quite smooth down to the separating points, without running the risk of a separation, or an eventual perturbation at the front shoulders (the points where the front elliptical arc touches the upper and lower flat plates) (Bearman, 1965).

3. NUMERICAL STRATEGY

The numerical code, named Incompact3d, a multi-purpose code for incompressible flows, was developed in its basic configuration by Lamballais and Silvestrini (2002). This code is capable of solving the two- and three-dimensional incompressible Navier-Stokes equations by means of DNS (Direct Numerical Simulation). The main characteristics of Incompact3d are listed below:

- The code is of the Poisson-type — see Ferziger and Perić (2002), running on a co-located grid. (In addition, an

advection-diffusion equation for a passive scalar is aggregated to the modelling.)

- The advancement in time is realized by means of a third-order low-storage Runge-Kutta strategy proposed by Williamson (1980). Part of the forcing terms in the immersed boundary sub-routine are advanced implicitly, instead, and the Crank-Nicolson scheme is used. This feature improves the efficiency of the forcing mechanism (Fadlun $et\ al.$, 2000; Lamballais and Silvestrini, 2002).
- The spatial derivatives are approximated by a sixth-order compact finite-difference scheme proposed by Lele (1992).
- The boundary condition at the solid surfaces is simulated using the immersed boundary technique, developed by Goldstein, Handler and Sirovich (1993). This method employs a feedback forcing to impose the no-slip condition at immersed boundaries present in the fluid domain. The external imposed force, that may vary in space and time, has to oppose the magnitude and direction of the local flow effect. A remarkable advantage of this method is the possibility of discretization on an uniform grid.
- The integrated hydrodynamical forces are solved using the control volume technique.

Incompact3d has already been tested in a series of applications to flows of interest, such as:

- Complex simulations of the wake flow behind a circular cylinder, including the interference of a mixing layer and oblique shedding (Silvestrini and Lamballais, 2004 and Lamballais and Silvestrini, 2002.
- Two-dimensional flow around bluff bodies (Ortega, Girardi and Silvestrini, 2007, Ribeiro, 2002 and Molina and Silvestrini, 2008.
- Transition to turbulence in the mixing layer using DNS and LES (Martinez, 2006.).

DNS of bluff body wake problems has received a great deal of attention, as a consequence of outstanding progresses in computational power and algorithm development. The DNS solves the Navier-Stokes equations for all flow scales, without any turbulence closure equations, leading, normally, to high computational costs. Nowadays, not only are the mean parameters such as Strouhal number, drag force, base pressure, and stresses in the wake well predicted, but the simulations provide complete flow field data banks, which enables one to better comprehend the physics of the flow (Wiliamson, 2006).

4. EXPERIMENTAL APPARATUS

The experiments were conducted in a low-speed wind tunnel at Laboratory Feng, Technological Institute of Aeronautics (ITA). The wind tunnel is an open circuit design with a square working section ($101.6mm$ x $101.6mm$) and a length of $190.0mm$. The facility operates at flow speeds (U_∞) of $1m/s$ to $32m/s$ and a turbulence level of approximately 0.5%. The tunnel pressure tappings were located at the beginning of the suction area (approximately the total pressure) and at the beginning of the working section (static pressure).

A commercial (Dantec) fibre-optic LDA-system arranged in back-scatter mode was employed (focal length, $800mm$). For measurements of the streamwise (U) and cross-wise (V) velocity components, respectively, the green (wavelength $514.5nm$) and the blue ($488nm$) coherent lights of an argon-ion laser was used. The signals of the photomultipliers were analysed using the BSAFlow Software. The seeding was provided by a oil-based fog generator, placed outside the tunnel so that the fog would diffuse before entering the tunnel. This avoided large concentrations of particles entering the laser plane. The computer-controlled 2D-traverse system had a positional accuracy of about $0.01mm$ with a resolution of about $0.005mm$.

At previous runnings, the boundary-layer thickness at the mid-station of the working length was measured and the result was approximately $8mm$. Thus, end-plates were attached at $10mm$ from either wall to reduced the inflow from the wind tunnel boundary layer to the low pressure region behind the model. The end plates were designed following recommendations by Stansby (1974). They were rectangular shaped plates $10.1h$ height, $16.0h$ long and the distance between body axis and the leading edge of end-plate was $7.0h$. Both the end plates and the parallel-sided sections of the model are made of aluminium, while the frontal half-ellipse is made of wood.

Unless otherwise stated, all distances and lengths are scaled by the body base height (h), velocities by the free stream velocity ($U\infty$), and frequencies by (U_∞/h). The origin of the coordinate system was placed at the body-base-height mid-point (midspan position). The streamwise, crosswise and spanwise directions are denoted x,y and z, respectively. The wake centerplane ($y = 0$) was found from symmetry of the measured streamwise velocity across the wake. The traverse system was then aligned with the intersection of this plane and a vertical mid-span streamwise plane ($z = 0$). After this procedure, the center of the body base ($x = 0$) was found from the two positions ($x = \pm 1/2$) where the laser beams touched the body surface.

5. RESULTS

In this section, a study of the blunt-trailing-edged body main parameters will be presented. An aspect that deserves to be noted is the difference between the number of points per base height in both Cartesian grids. In the 2-D case (DNS), we have used 30 points per base height in the cross-wise direction and 25 points per base height in the streamwise direction, the 3-D case (DNS) has 16 points in all directions with the spanwise length of $8h$. While for the 3-D case (LDA), we have used 10 points per base base height in both directions excepted in the boundary-layer and shear layer regions where the mesh were refined. One should keep in mind that experimental simulations are very costly, each point last approximately 60 seconds to be measured. This should explain the difference between the numerical and the experimental ("discreet") velocities fields. Thus, the reader is invited to appreciate Figs 2 and 3 where we compare for the same Reynolds Number and aspect ratio the velocities fields, even with the differences discussed previously, the topology of the flow agrees qualitatively in each comparison presented.

A summary of the critical values from DNS simulations and LDA-measurements for $AR = 3$ at a same Reynolds number ($Re = 600$) is compiled in Table 2. The mean streamwise, mean cross-wise, RMS streamwise velocities fields and Reynolds Stresses are presented in Figs. 2 and 3, respectively. The underlying data is depicted in Fig. 6. The mean streamwise velocity $U(x, 0)$ showed a consistent decrease towards zero when approaching the base of the body ($x = 0$). The RMS streamwise-velocity component, U_{rms}, followed the same pattern of decrease.

	Re	l_c	U_{min}	l_f	U_{rms}	δ	θ	St	$\Gamma/U_\infty h$
DNS (2-D)	600	0.60	-0.20	0.57	0.72	0.098	0.028	0.236	3.479
DNS (3-D)	600	0.87	-0.20	-	-	0.099	0.038	0.248	3.106
LDA	600	1.15	-0.22	1.05	0.34	0.105	0.035	0.222	4.080

Table 2: Summary of the critical values

First of all, it is important to inform that the concept of vortex formation length, l_f, that was used to obtain the results appearing in Fig. 6b is the one adopted in the works of Bearman (1965), see also Williamson (1996). The formation length is the distance to the body base of the streamwise-velocity fluctuation peak (RMS value) at $y = 0.25$. The value of the wake closure length, l_c, was about 49% lower in the DNS simulation, Fig. 6a. The same value was found for the vortex formation length.

The shorter vortex formation length in the DNS simulations is associated to the higher Reynolds stress ($\bar{u'v'}$) being closer to the body in the 2-D case (when compared to the 3-D case) as stated by Mittal and Balachandar (1995) for a circular cylinder. The reader can observe in Figs. 3b and 3d the difference between both maximum values confirming what was stated, also for the blunt-trailing-edged body. From Fig. 3d it was found that the Reynolds stress is small everywhere on the separation streamline and attain large values inside the core of the separation bubble. Furthermore, the increase in the 2-D Reynolds stress is also connected to the diminishing of the pressure at the base region, what translates in a two-dimensional larger drag, a result well known in the literature and presented in Tab. 3 . Physically, and in general terms, what happens is that in a three-dimensional situation the flow is offered an "alleviation" by the presence of the spanwise space. The above results are consistent with the decrease in Reynolds stresses for the 3-D flow, found also by Karniadakis and Triantafyllou (1992) (see also Ortega, Girardi and Silvestrini, 2009). The RMS streamwise velocity field shown in Figs. 3a for the 2-D case are also found to be significantly higher in magnitude than the corresponding 3-D case, Fig. 3c. In addition, the DNS (3-D) mean lift RMS coefficient is higher in value than the correponding DNS (2-D) case as shown in Tab. 3.

	Re	C_{pb}	C_d	$C_{l_{rms}}$
DNS (2-D)	600	-1.148	1.142	0.976
DNS (3-D)	600	-0.655	0.824	0.314
LDA	600	-0.816	-	-

Table 3: Comparison of the base pressure coefficient and the mean drag and lift coefficient.

The agreement between simulation and experiment is good for the Strouhal number, base pressure coefficient and the tip boundary layer displacement and momentum thickness. The reader should bear in mind that the aspect ratio is equal to 3 and the Reynolds number is 600. For this value of the Reynolds number, the boundary layer is laminar and the profile agrees very well with the Blasius laminar solution for the flat plate (not shown on this paper) also, the wake after the body is eminently three-dimensional, considering transition to turbulence (modes A and B has already manifested) (Ryan, Thompson and Hourigan, 2005; Ortega, Girardi and Silvestrini, 2009), as shown in Fig. 4. These effects, evidently three-dimensional, do not appear in the two-dimensional simulations. Some comments should be made about results from the

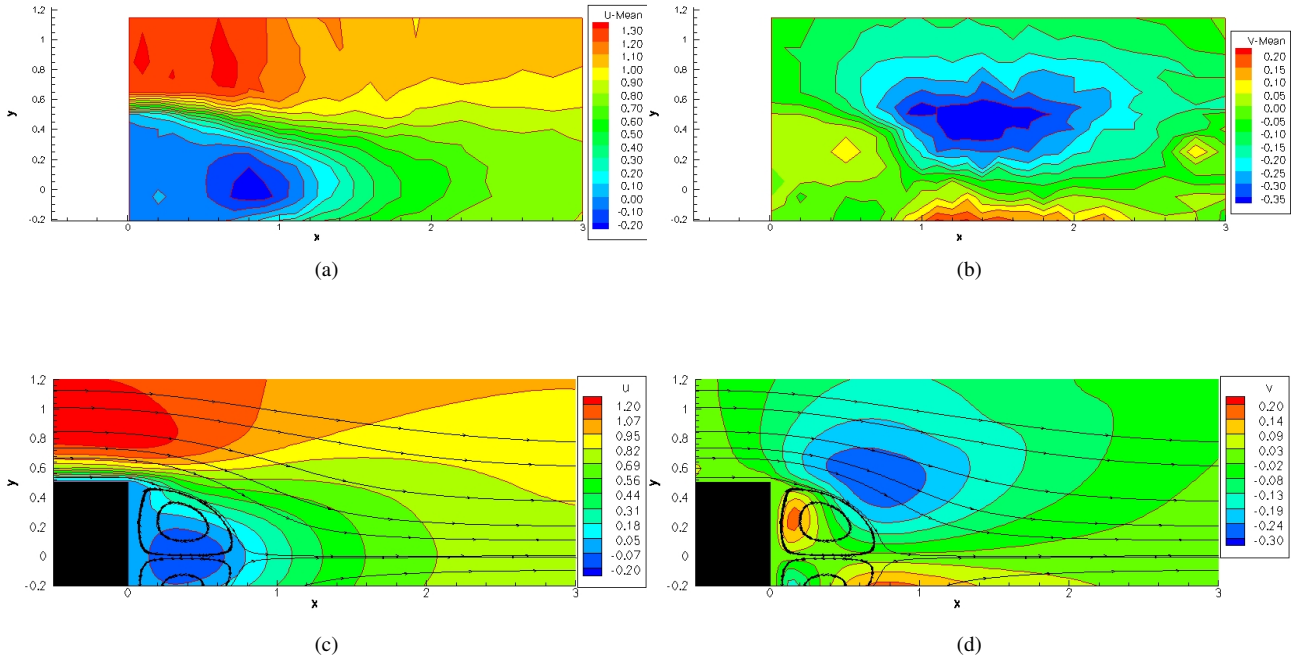

(a) (b)

(c) (d)

Figure 2: Mean streamwise velocity field, AR=3 and Re=600: (a) LDA, (c) 2-D DNS. Mean cross-wise velocity field: (b) LDA, (d) 2-D DNS

2-D DNS. It is well known that the 2-D assumption can lead to an unrealistic flow. In a consequence, the 2-D DNS should be view as a reduced model where 3-D motions are artificially prevented (Lamballais, Silvestrini and Laizet, 2010). This point is illustrated in Figs. 5a and 5b where the occurrence of a turbulence breakdown destroy the 2D coherence of the large scale structure as they travel downstream. A more complete view of the 3-D dynamics can be obtained by volume visualization of a characteristic vorticity isosurface as presented in Fig. 4.

The fact that we got good agreement in the case of the pressure coefficient is because we have used data at the separation point boundary layer, Fig. 6c. In other words, we relied on the values of K and not on the usual pressure coefficient definition formula. The mean circulation (Γ) that leaves the body during the release of a single vortex can be dimensionless using the Strouhal number (St) and the rate (K) in accordance with Eq. (3).

$$\frac{\Gamma}{U_\infty h} = \frac{K^2}{2St} \tag{3}$$

where h is the body height. But, this value of circulation is not necessarily the one encountered downstream in a single vortex, what is a consequence of a certain amount of dissipation due mainly to interactions between the growing vortices at the formation region.

Some notable features were found from plots of the streamwise and cross-wise velocities in the shear layer of the blunt-trailing-edged body, as shown in Fig. 6d. There is an increase in the streamwise component and inversely, a decrease in the cross-wise component up to the wake closure length, l_c, for both simulations then, the cross-stream velocities increase until zero. On the other hand, the 3-D streamwise component slowly increases towards 0.85. Although the simulated streamwise velocity presented a different pattern of increase, the final value was the same for both simulation and experiment. Possibly, the entrainment from outside the shear layer to the wake is maximum at the point where the cross-wise velocity is more negative.

6. Conclusions

The first results of a research work that deals with experimental (LDA) three-dimensional and numerical (DNS) bi-dimensional flows around a blunt-trailing-edged body are presented and discussed. The basic aim is to compared the presenting data with the literature mostly, the circular cylinder. In general, results are quite good and compares very well. The shorter formation length, l_f, and the wake closure length, l_c, were found in the 2-D case, as was stated for the circular cylinder, due to higher Reynolds stress values in magnitude. The study is not finished yet, in fact it is in the beginning, there remain others aspect ratios to be studied. Also, it is very important to investigate the influence of the boundary layer development, spectral and instantaneous fields analysis where, much probably, other differences will show up.

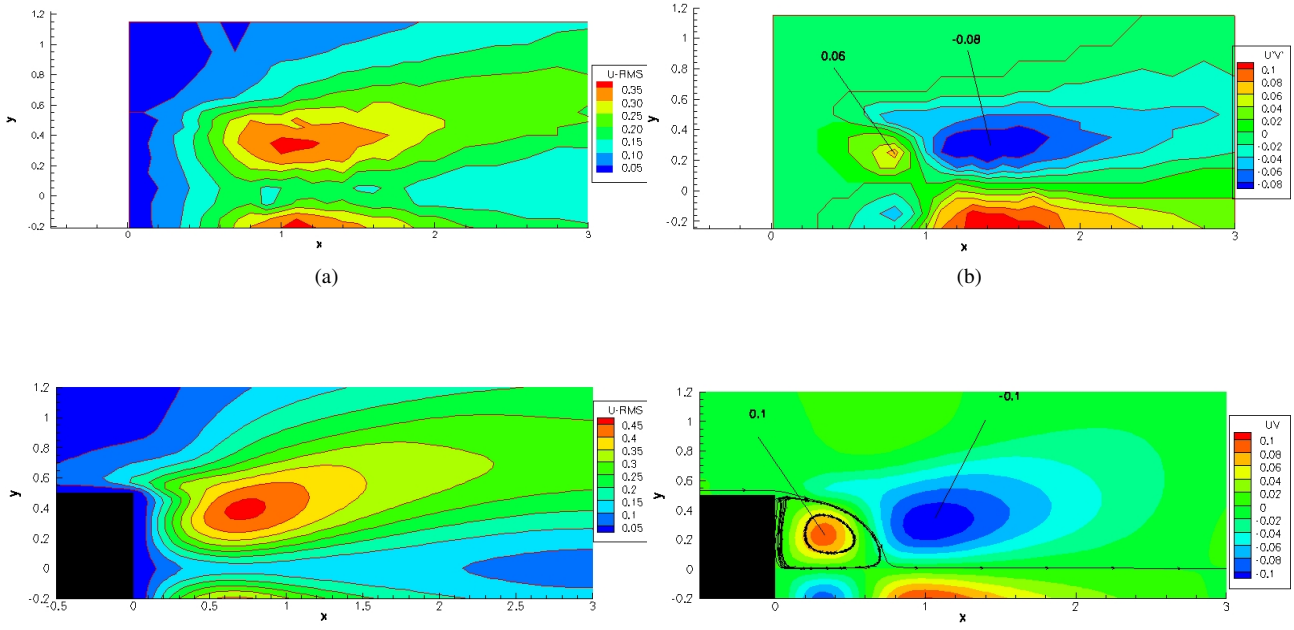

(a) (b)

(c) (d)

Figure 3: RMS velocity field, AR=3 and Re=600: (a) LDA, (c) 2-D DNS. Reynolds Stress: (b) LDA, (d) 2-D DNS

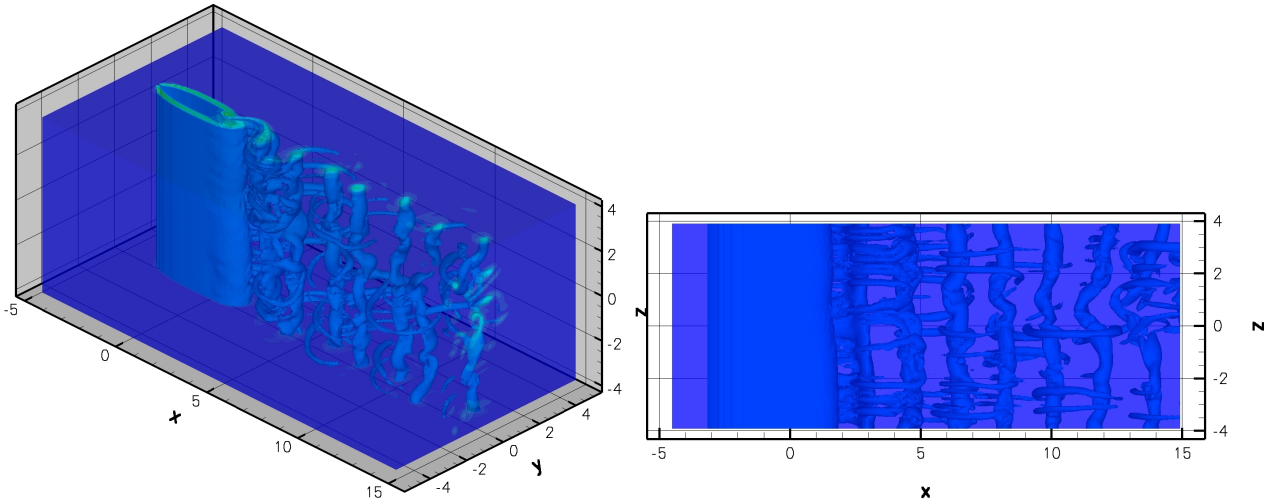

(a) (b)

Figure 4: (a) Perspective view of vorticity modulus isosurface $\omega = 3.2$; (b) Top view of vorticity modulus isosurface $\omega = 3.2$.

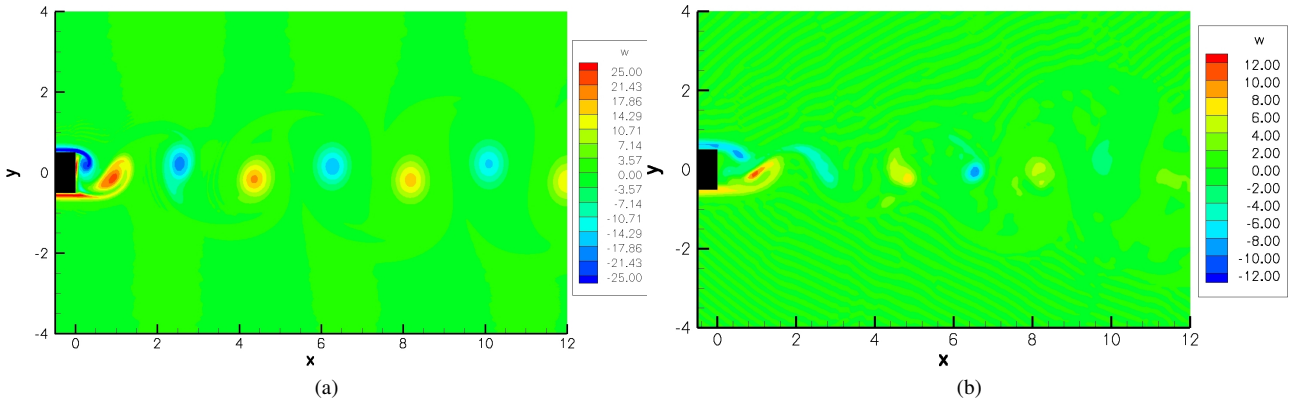

(a) (b)

Figure 5: Maps of spanwise vorticity ω_z: (a) 2-D DNS and (b) 3-D DNS.

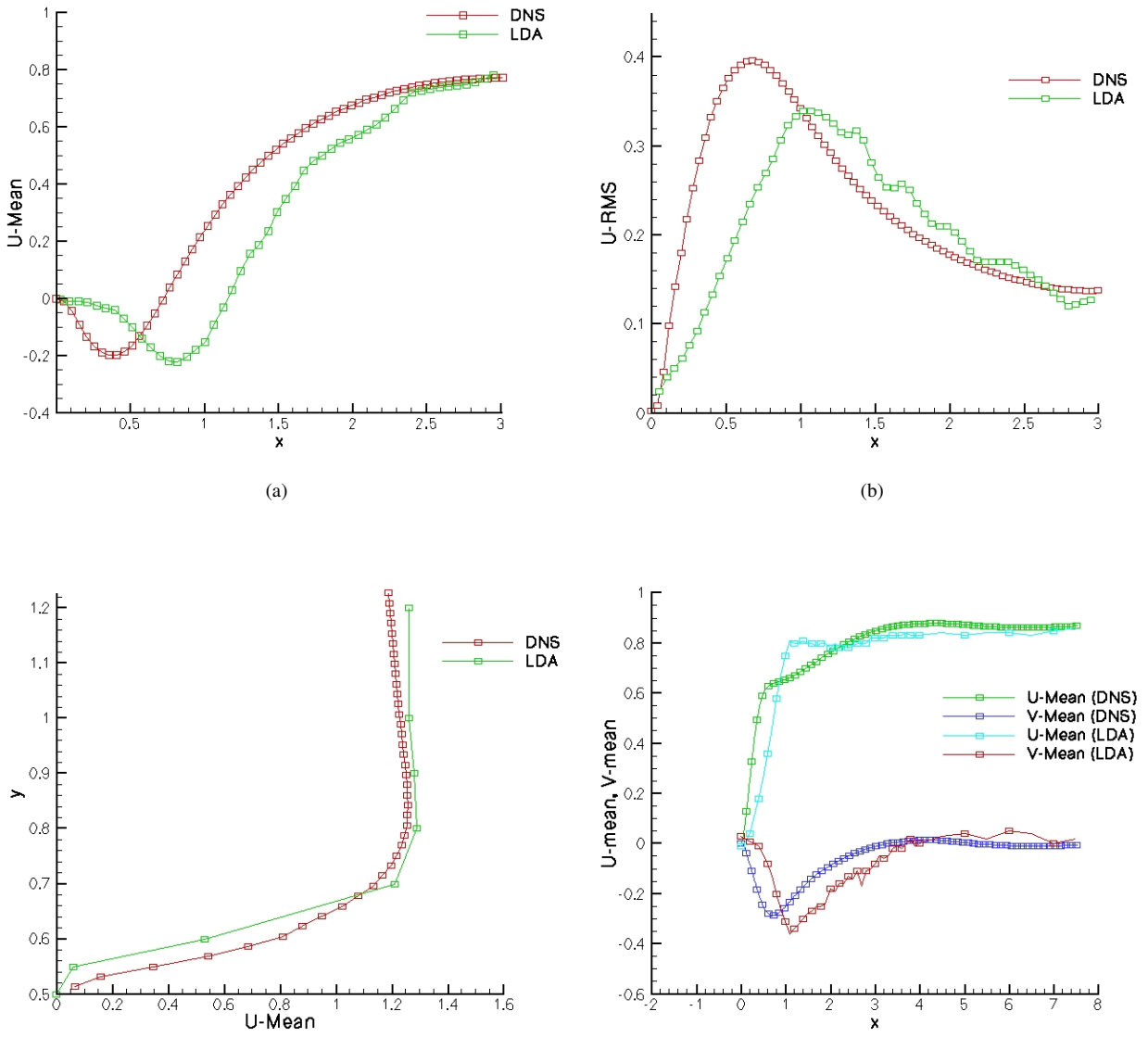

Figure 6: Results from 2-D (DNS) and 3-D (LDA) simulations, AR=3 and Re=600. (a) mean streamwise velocity along the wake centerline, (b) RMS streamwise velocity along $y = 0.25$, (c) boundary layer profile, (d) mean streamwise velocity along $y = 0.5$

7. ACKNOWLEDGEMENTS

The authors would like to acknowledge the financial support provided by CNPq, the Brazilian National Council of Research and Development, through grant 303184/2007-8, and Fapesp, the State of São Paulo Foundation for the Support of Scientific Research, through grant SP/2549/2007. The authors are grateful to Prof. Jorge Hugo Silvestrini for his precious advices on this work.

8. REFERENCES

Bearman, P.W., "Investigation of the flow behind a two-dimensional model with a blunt trailing edge and fitted with splitter plates". J. Fluid Mech., 21:241-255, 1965.

Bloor,M.S., "The transition to turbulence in the wake of a circular cylinder". J. Fluid Mech., 19:290-304, 1964.

Fadlun, E.A., Verzico, R., Orlandi,P. and Mohd-Yusof,J., "Combined immersed-boundary finite-difference methods for three-dimensional complex flow simulations." J. Comp. Phys., 161:35âĂŞ60, 2000.

Fage, A. and Johansen, F.C., "The structure of vortex sheets." Proc. Roy. Soc. Lond. A, 1928.

Ferziger, J.H. and Perić,M., "Computational Methods for Fluid Dynamics", Springer Verlag, Berlin, 2002.
Gerrard, J.H., "The mechanics of the formation region of vortex behind bluff bodies." J. Fluid Mech., 25:401-413, 1966.
Goldstein, D. , Handler, R. and Sirovich, L., "Modeling a no-slip boundary condition with an external force field." J. Comp. Phys., 105:354-366, 1993.
Kamiadakis, G.E., Triantafyllou, G.S., "Three- dimensional dynamics and transition to tur- bulence in the wake of bluff objects." J. Fluid Mech. 238:l, 1992.
Lamballais, E. and Silvestrini, J.H., "Direct numerical simulation of interactions between a mixing layer and a wake around a cylinder." J. Turbulence, 3(28):1-21, 2002. ïż£
Lamballais, E., Silvestrini, J.H., Laizet, S., "Direct numerical simulation of flow separation behind a rounded leading edge: Study of curvature effects." Int. J. of Heat and Fluid Flow.;31(3):295-306, 2010.
Lele, S.K., "Compact finite difference schemes with spectral-like resolution". J. Comp. Phys., 103:16-42, 1992.
Mittal, R. and Balanchadar, S., "Effect of three-dimensionality on the lift and drag of nominally two-dimensional cylinders.", Phys. Fluids, 7(8):1841-1865, 1995.
Molina, E.S and Silvestrini, J.H., "Simulação numérica de um escoamento ao redor de um par de cilindros em tandem com oscilação forçada". In VI Escola de Primavera de Transição e Turbulência, São Carlos, 2008.
Ortega, M., Girardi, R. and Silvestrini, J.H., "The formation region behind a blunt body fitted with splitter plate.", AIAA Paper,132-2007, 2007.
Ortega, M., Girardi, R. and Silvestrini, J.H., "The topology of three-dimensional flows about blunt bodies for low values of the Reynolds Number.", Proceedings of the 20th Brazilian Congress of Mechanical Engineering, Gramado, Brazil, 2009.
Ribeiro, P., "Desprendimento de vórtices e controle de esteira de cilindros por simulação numérica direta". Dissertação de mestrado em Recursos Hídricos e Saneamento Ambiental, Universidade Federal do Rio Grande do Sul, 2002.
Roshko, A., "On the development of turbulent wakes from vortex streets". NACA Report, 1954.
Roshko, A., "On the drag and shedding frequency of two-dimensional bluff bodies". NACA Report, 1954.
Roshko, A., "Perspectives on bluff body aerodinamics. J. of Wind Engineering and Industrial Aerodynamics", 49:79-100, 1993.
Ryan, K., Thompson, M.C. and Hourigan, K., "Three-dimensional transition in the wake of bluff elongated cylinders". J. Fluid Mech., 538:1-29, 2005.
Silvestrini, J.H. and Lamballais, E., "Direct numerical simulations of oblique vortex shedding from a cylinder in shearflow". Int. J. Heat and Fluid Flow, 25:461-470, 2004.
Stansby, P.K., "The effect of end plates on the base pressure coefficient of a circular cylinder". R. Aeronaut. J., 78:36-37, 1974.
Strouhal V. 1878. Uber eine besondere Art der Tonerregung. Ann. Phys. Chem. (Liepzig), Neue Folge Bd. 5:216, Heft 10
Szepessy, S. and Bearman, P.W., "Aspect ratio and end plate effects on vortex shedding from a circular cylinder." J. Fluid Mech., 234:191-217, 1992.
Williamson, C.H.K., "Vortex dynamics in the cylinder wake. Annu. Rev. Fluid Mech.", 28:477-539, 1996.
Williamson, J. H. "Low-storage Runge-Kutta schemes." J. Comp. Phys., 35:48-56, 1980.

9. Responsibility notice

The author(s) is (are) the only responsible for the printed material included in this paper.